Renewable and Sustainable Energy Reviews 131 (2020) 109995

Contents lists available at ScienceDirect

Renewable and Sustainable Energy Reviews

journal homepage: http://www.elsevier.com/locate/rser

Low-emission pre-combustion gas-to-wire via ionic-liquid [Bmim][NTf_2] absorption with high-pressure stripping

Hudson Bolsoni Carminati [a], José Luiz de Medeiros [a,*], Gustavo Torres Moure [b], Lara Costa Barbosa [a], Ofélia de Queiroz F. Araújo [a]

[a] Escola de Química, Federal University of Rio de Janeiro, CT, E, Ilha Do Fundão, Rio de Janeiro, RJ, 21941-909, Brazil
[b] CENPES, PETROBRAS, Ilha Do Fundão, Rio de Janeiro, RJ, 21941-598, Brazil

ARTICLE INFO

Keywords:
Autothermal reforming
Hydrogen
Gas-to-Wire
Pre-combustion
Ionic-liquid
CCS

ABSTRACT

Autothermal reforming is an important pathway to hydrogen via fossil fuel decarbonization. Traditionally, the finishing step of hydrogen production via autothermal reforming consists of decarbonation via conventional aqueous-amine absorption which incurs a huge energy penalty due to high heat-ratio and low-pressure carbon dioxide stripping entailing costly compression for geological storage. This work proposes and assesses an alternative high-pressure temperature-swing hydrogen decarbonation that promotes stripping at high-pressure reducing carbon dioxide compression costs. Such new hydrogen decarbonation uses 1-Butyl-3-methylimidazolium bis(trifluoromethylsulfonyl)-imide ionic-liquid physical-absorption due to its solute affinity, low vapor-pressure, high thermal stability and low heat consumption for carbon dioxide stripping at high-temperature and high-pressure. Technical and economic aspects of the ionic-liquid temperature-swing decarbonation are evaluated and compared with the conventional aqueous-amine decarbonation. Results showed that high-pressure ionic-liquid stripping requires *5.5* times less heat to produce a high-pressure carbon dioxide stream and reduces *4.3* times its compression power. These results directly impact net power exportation of the combined-cycle hydrogen-fired power plant; i.e., the ionic-liquid gas-to-wire exports *35.6%* more electricity than the aqueous-amine counterpart. Economically, the ionic-liquid gas-to-wire has *36%* higher revenues, entailing a net value *2.5* times higher (US$ *390.2*10^6*) and 5 years lower payback-time than the conventional aqueous-amine counterpart.

1. Introduction

The increasing demand for energy supply drives worldwide the development of alternative sources as well as the efficiency improvement of established technologies. In this context, natural gas (NG) reforming has received attention as a technically feasible bridge from fossil NG to hydrogen (H_2), a promising carbon-free fuel [1]. NG reforming produces hydrogen via synthesis-gas (syngas) conversion [2] and NG is the principal fossil source for syngas production due to its wide availability and high methane content. Around *90%* of H_2 world production is obtained through NG reforming [3].

The two main pathways for methane reforming are steam-reforming and dry-reforming. The latter uses carbon dioxide (CO_2) as conversion agent, being useful to improve CO/H_2 ratio, while steam-reforming is the most widespread method for large-scale syngas production [4]. Nevertheless, a combination of steam-reforming and dry-reforming can be used to produce syngas with a desirable H_2/CO ratio [5]. Methane reforming has been investigated to improve energy efficiency of fuel-fired power plants, as occurs in thermochemical waste-heat recovery. In this method, the heat of reformer gases is converted into chemical energy of a decarbonized fuel with a superior lower-heating value [6]. The use of thermochemical recovery is increasing in power plants and emphasizes the importance of improving hydrocarbon reforming

Abbreviations: ATR, Autothermal Reforming; [Bmim][NTf_2], 1-Butyl-3-methylimidazolium bis(trifluoromethylsulfonyl)-imide; CW, Cooling-Water; EOR, Enhanced Oil Recovery; GT, Gas-Turbine; HPL, High-Pressure Liquid; HPS, High-Pressure Steam; HRSG, Heat-Recovery-Steam-Generator; HT, High-Temperature; IL, Ionic-Liquid; LT, Low-Temperature; MPL, Medium-Pressure Liquid; MPS, Medium-Pressure Steam; MEA, Monoethanolamine; MMSm^3/d, Million Standard m^3/d; MMUSD, Million US Dollars; NG, Natural Gas; PCC, Pre-Combustion Capture; PR-EOS, Peng-Robinson Equation-of-State; RK-EOS, Redlich-Kwong Equation-of-State; Syngas, Synthesis-Gas; VLE, Vapor-Liquid Equilibrium; WGS, Water-Gas Shift.

* Corresponding author.
E-mail address: jlm@eq.ufrj.br (J.L. de Medeiros).

https://doi.org/10.1016/j.rser.2020.109995
Received 9 January 2020; Received in revised form 10 June 2020; Accepted 11 June 2020
Available online 29 June 2020
1364-0321/

Nomenclature

AP	Net annual-profit (MMUSD/y)
C_{BM}	Bare module cost (USD)
COL	Cost of labor (MMUSD/y)
COM	Cost of manufacturing (MMUSD/y)
C_p	Gas isobaric heat capacitiy (J/mol.K)
C_p^{ig}	Ideal gas isobaric heat capacity (J/mol.K)
CR	Capture-Ratio ($kg^{Solvent}/kg^{CO2}$)
CUT	Cost of utilities (MMUSD/y)
DEP	Depreciation (MMUSD/y)
FCI	Fixed capital investment (MMUSD)
f_i^0	Standard-state fugacity of species i (bar)
$\widehat{f}_i^L$	Liquid fugacity of species i (bar)
$\widehat{f}_i^V$	Vapor fugacity of species i (bar)
GAP	Gross annual-profit (MMUSD/y)
H_i	Ionic-liquid Henry constant of species i (bar)
HR	Heat-Ratio (kJ/kg^{CO2})
i	Annual interest rate (%)
N	Operational years (y)
NPV	Net present value (MMUSD)
P	Pressure (bar)
REV	Revenues (MMUSD/y)
T	Absolute temperature (K)
T_c	Critical temperature (K)
T_r	Reduced temperature
x_i	Liquid mole fraction of species i
y	Vapor mole fraction of species i
$\widehat{\gamma}_i^L$	Liquid activity coefficient of species i
$\widehat{\varphi}_i^V$	Vapor fugacity coefficient of species i

processes.

The transition from fossil fuels to H_2 emerges not only as an energy strategy, but also as an important step towards low-carbon energy production enabling to associate fuel switching with carbon capture and storage (CCS) [7]. Electricity generation via H_2-fired power plants can be considered a cleaner process if properly integrated to CCS. Thus, for logistical reasons, the implementation of NG reforming integrated to H_2-fired power plant can be convenient for remote oil-gas fields (e.g., deep-seawater fields), enabling to use captured CO_2 as enhanced oil recovery (EOR) agent in the same field minimizing CO_2 pipeline costs [8]. This integration is a gas-to-wire (GTW) facility receiving NG from the field and exporting electricity through long-distance high-voltage cables. GTW has the additional advantage of avoiding complex pipelines for NG exportation vis-à-vis electricity transmission lines [9].

Methane steam-reforming is a widespread catalytic process to obtain syngas from light hydrocarbons [10] whose endothermic reactions are favored by elevated temperatures, promoted through burning NG externally [11]. The problematic dependence of external heat supply can be overcome by partial oxidation, which occurs by burning NG with oxygen at sub-stoichiometric ratios, producing syngas, a mixture of carbon monoxide (CO) and H_2 [12].

Alternatively, when steam is fed into an adiabatic NG reformer with air there is a competition between reforming and partial oxidation reactions. The combination of the endothermic methane steam-reforming with the exothermic partial oxidation in an autonomous way characterizes the autothermal reforming (ATR) [13]. ATR entails the following benefits: (i) lower footprint and investment; (ii) short startup periods and fast load changes; and (iii) syngas suitable for downstream applications [14].

Likewise other pre-combustion processes, a major ATR challenge is the removal of undesirable components from syngas such as CO_2 [15]. Several alternatives exist for syngas decarbonation in both pre-combustion/post-combustion concepts. For CO_2–H_2 separation in applications with chemical synthesis – e.g., NH_3 synthesis, wherein CO_2 is highly undesirable – new operations can promote a high H_2 purity; e.g., molecular-sieves adsorption and membrane-permeation [16]. However, these modular and practical technologies are more attractive at lower scales and may entail high costs for high-scale plants. In addition, CO_2 separation from syngas for H_2-fired power plants does not need such high purity requirements. H_2-fired power plants only require some CO_2 capture (say, abatement of ≈90% of CO_2) such that flue-gases are released with low CO_2 content (i.e., below ≈3%mol). In other words, high-scale chemical or physical absorptions are appropriate [17] for syngas treatment in H_2-fired power plants. Aqueous-amine chemical-absorption is a widespread gas decarbonation technology with long-term commercial utilization and satisfactory large-scale performance [18]. Nevertheless, aqueous-amine decarbonation has some shortcomings such as high heat-ratio CO_2 stripping, thermal degradation, corrosiveness and low-pressure final CO_2 [19].

Studies have been conducted to substitute aqueous-amines by alternative solvents with better thermal/chemical stability, lower corrosiveness, lower regeneration heat-ratio and high-pressure CO_2 release [20]. In this context, physical solvents appear as attractive solutions to accomplish CO_2 capture, especially at high CO_2 partial pressure (fugacity) [21]. The main advantage of physical-absorption relies on the lower heat-ratio for CO_2 stripping due to weak solvent-CO_2 physical interaction. The physical-absorption Selexol process has been considered a feasible alternative to membrane-permeation for NG decarbonation [22]. Other potential physical solvents for high-pressure NG decarbonation are encountered in the ionic-liquid (IL) category of species [23].

1.1. Ionic-liquids for gas decarbonation

Recently, ILs have attracted attention as promising substitutes to conventional solvents for CO_2 capture. Some ILs have highly desirable characteristics such as high thermal/chemical stability, high CO_2 solubility, low volatility and low heat-ratio for CO_2 stripping [24]. Moreover, some ILs have shown superior CO_2 selectivity when compared to other gases (e.g., CO, H_2, and O_2). In certain ILs CO_2 solubility is higher comparatively to the solubility of N_2 and H_2, which make them suitable to perform high-pressure shifted-syngas decarbonation [20].

ILs have been investigated in the literature as solvents for CO_2 capture. The application of IL [Bmim][Ac] for post-combustion capture was investigated by Shiflett et al. [25] who reported a *16%* reduction of heat demand with higher CO_2 purity relative to conventional aqueous-monoethanolamine (MEA) absorption, besides lower capital investment (*11%*) and equipment footprint (*12%*). Liu et al. [26] assessed two alternatives for shale-gas decarbonation using [Bmim][NTf_2] under single and multi-staged pressure-swing IL stripping, showing *42.8%* and *66.04%* reduction of heat consumption, respectively. IL [Bmim][NTf_2] was also used for CO_2 capture in power plants by Ma et al. [27] saving *30%* of heat consumption.

Zubeir et al. [28] in a simulation study compared IL [C_6mim][TCM] and Selexol for CO_2 pre-combustion capture (PCC) from synthetic NG showing that IL absorption has higher CO_2/CH_4 selectivity than Selexol. The authors recommended a combination of pressure-swing and temperature-swing for IL stripping. Pressure was reduced to *9.*2 bar in the last flash reducing the recompression costs considerably relatively to using pressure-swing at 1 bar as the absorber operates at 28 bar.

Barbosa et al. [29] proposed a new processing of CO_2-rich NG using IL [Bmim][NTf_2] for simultaneous CO_2 removal, water and hydrocarbon

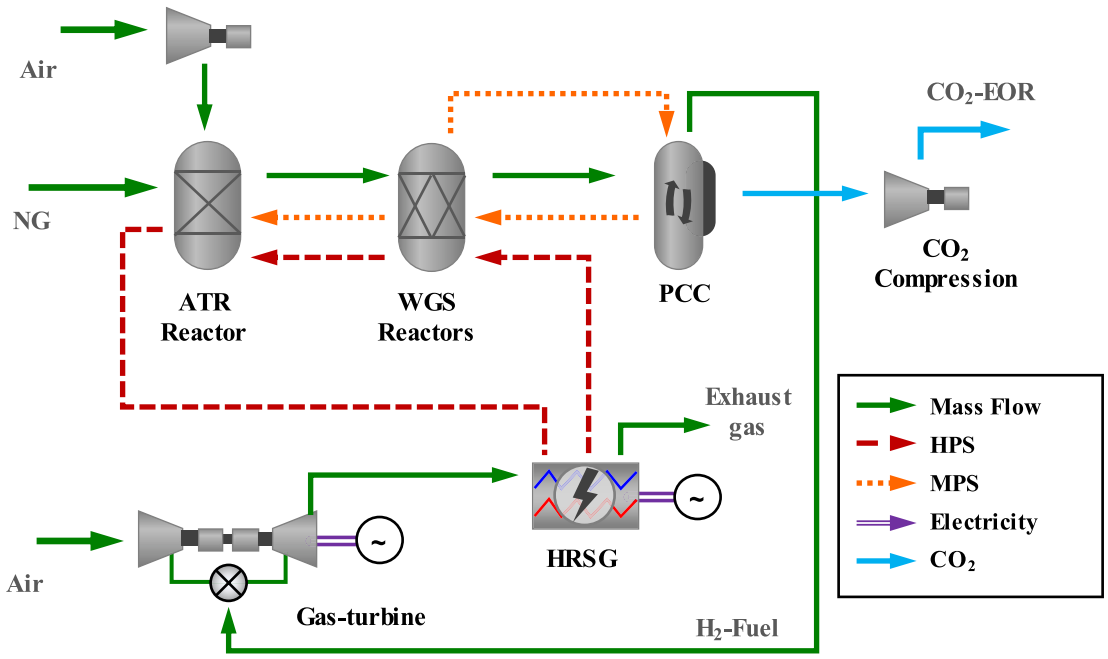

Fig. 1. Low-emission ATR-GTW process integrated to PCC plant.

dew-points adjustment. Simulation showed that the high-pressure selective stripping of CO_2 provided by IL entails lower CO_2 compression costs for EOR applications. Such new IL-based NG processing showed better revenues and manufacturing cost, giving a net value *37%* higher than the NG processing via conventional aqueous-amine decarbonation and conventional dew-points adjustment.

As seen above, the literature has explored new IL-based gas decarbonation processes focusing mainly on NG sweetening and processing. On the other hand, there is an absence of studies on pre-combustion CO_2 capture via IL absorption coupled to ATR as a route to H_2 production. This is a clear literature gap to explore, given the increasing interest on H_2 as a clean fuel.

1.2. The present work

A low-emission gas-to-wire facility integrating NG autothermal reforming to H_2 combined-cycle (ATR-GTW) is presented. It is proved that ATR-GTW emerges as a promising clean power production concept using a new temperature-swing CO_2 absorption with the IL 1-Butyl-3-methylimidazolium bis(trifluoromethylsulfonyl)imide ([Bmim][NTf_2]) as solvent for H_2-Fuel pre-combustion decarbonation. IL-based ATR-GTW is assessed on technical and economic grounds and compared to the conventional ATR-GTW via aqueous-MEA absorption with low-pressure stripping. Both processing routes are rigorously simulated in Aspen-Plus. Since IL is a new component in Aspen-Plus, implementation of accurate description of pure IL thermodynamic and transport properties is required for energy balances and equipment design (exchangers, pumps and columns). Accurate thermodynamic description of IL binary systems with the solutes of interest (H_2, CO_2, CO, N_2, O_2, H_2O, CH_4, C_2H_6) aiming at adequate representation of high-pressure vapor-liquid equilibrium (VLE) in absorption/stripping operations is necessary as well.

An innovative feature of such IL-based temperature-swing pre-combustion capture relies on CO_2 stripping at high-pressure and high-temperature taking advantage of the high thermal stability of IL and extremely low vapor-pressure. As a result, the new IL-based route entails remarkable reduction of CO_2 compression costs to meet the conditions of CO_2-rich fluid to EOR. Additionally, the high-pressure high-temperature CO_2 stripping from IL requires less heat consumption, increasing gas-to-wire power exportation. Given the absence of works in the literature focusing on NG reforming with IL pre-combustion capture, the present new low-emission ATR-GTW with IL syngas decarbonation fills this gap as a promising cleaner and economically more efficient power production route for remote oil-gas fields.

2. Methods

Technical, thermodynamic and economic aspects of ATR-GTW with PCC-IL and the conventional PCC-MEA counterpart were assessed through three steps: (i) design and simulation of processes, including LPS/HPS reallocation, CO_2 compression, and calculation of heat consumptions and exportable electricity; (ii) technical analysis; and (iii) economic assessment of ATR-GTW with PCC-IL and the PCC-MEA counterpart. Both ATR-GTW plants were simulated in Aspen-Plus 10 for solving mass-energy balances. Peng-Robinson Equation-of-State (PR-EOS) with free-water is used for most unit operations, excepting for PCC simulations, where specific models were selected (Table 4).

2.1. Technical background

Theoretical, modeling and simulation aspects are discussed as follows.

2.1.1. Autothermal reforming pre-combustion combined-cycle gas-to-wire plant

Fig. 1 depicts a low-emission ATR-GTW process integrated to a PCC plant for syngas decarbonation. High-pressure steam (HPS) and medium-pressure steam (MPS) are generated using heat from ATR reactor, from water-gas shift (WGS) reactors and from heat-recovery-steam-generator (HRSG) [30]. PCC plant consumes MPS for CO_2 stripping. The process comprises the following operations: (i) air compression; (ii) ATR reactor; (iii) WGS reactors; (iv) PCC; (v) CO_2 compression; (vi) H_2-fired gas-turbines (GT) with electric generators; and (vii) HRSG coupled to a Rankine-Cycle running steam-turbines with electric generators.

The ATR plant is fed with high-pressure desulfurized NG with low CO_2 content. NG is preheated and feeds the ATR reactor at 60 bar, a sufficiently high-pressure to prove the functionality of IL decarbonation,

Table 1
Constant properties of [Bmim] [NTf_2].

Property	Unit	Value
Boiling-Point (T_B)	*K*	*739.3*
Critical Temperature (T_C)	*K*	*1081.4*
Critical Pressure (P_C)	*bar*	*21.7*
Critical Volume (V_C)	*cm^3/mol*	*969.9*
Molecular Weight (MW)	*g/mol*	*419.36*
Acentric Factor (ω)	-	*0.2316*

Source: Barbosa et al. [29].

Table 2
Temperature-dependent properties of IL [Bmim] [NTf_2].

Property	Unit	Formulas with T(K)
Liquid Density (ρ)	*kg/m^3*	$\rho = 1719 - 0.946T$
Liquid Viscosity (μ)	*Pa.s*	$\ln \mu = -93.46 + 7058.17/T + 11.72 \ln T$
Surface Tension (σ)	*mN/m*	$\sigma = 0.69(1-T_r)^{-39.057+133.346T_r-106.38T_r^2-78.28T_r^3}$
Liq. Isobaric Heat Capacity ($\overline{C}_p$)	*J/mol.K*	$\overline{C}_p = -58.96 + 3.45T - 4.18{*}10^{-3}T^2$
Liq. Thermal Conductivity (k)	*W/mK*	$k = -0.78 + 8.6{*}10^{-3}T - 2.69{*}10^{-5}T^2 + 2.78{*}10^{-8}T^3$
Ideal Gas Heat Capacity ($\overline{C}_p^{ig}$) [27]	*J/mol.K*	$\overline{C}_p^{ig} = 185.45 + 1.19162\,T - 6.221\,{*}10^{-4}T^2 + 7.86{*}10^{-8}T^3$

*$T_r = T/T_c$. Source: Barbosa et al. [29]; Ge et al. [35].

but ATR is also feasible at higher pressures, if necessary. NG is mixed in the reformer directly with air and saturated MPS.

The reformer comprises three zones: (i) the burner, where the gas feed is injected as a turbulent flame; (ii) the combustion zone, where exothermic partial oxidation occurs; and (iii) the catalytic zone, where the mixture from the combustion zone flows through a catalyst bed enabling reforming reactions [31]. Firstly, gas reacts with oxygen; then, the resulting gas goes through a reforming catalyst yielding raw-syngas. Heat generated in the combustion zone is utilized in the steam reforming zone producing a H_2:CO ratio of *2.5:1* [31]. Partial combustion and steam reforming reactions are presented in Eqs. (1) and (2):

$$CH_4 + 1/2O_2 \rightarrow CO + 2H_2 \quad (1)$$

$$4CH_4 + O_2 + 2H_2O \rightarrow 10H_2 + 4CO \quad (2)$$

Alternatively, if CO_2 is used via dry-reforming, a *1:1* H_2:CO ratio results via Eq. (3).

$$2CH_4 + O_2 + CO_2 \rightarrow 3H_2 + 3CO + H_2O + heat \quad (3)$$

The hot raw-syngas is mainly N_2, H_2, CO, CO_2 and H_2O. It is a feedstock for various synthesis processes, such as methanol and Fischer-Tropsch syntheses [32]. Here, syngas is an intermediate to produce decarbonized clean fuel for power generation, hence it is submitted to WGS reactors where H_2 content is increased via Eq. (4) consuming CO and H_2O [33].

$$CO + H_2O \rightarrow CO_2 + H_2 \quad (4)$$

At this stage, the purification of the high-pressure shifted-syngas aims only to remove CO_2 in the PCC, which can be conducted with aqueous-MEA absorption or, as proposed in the present work, with temperature-swing IL [Bmim][NTf_2] absorption. After PCC, the fuel-gas is basically N_2 and H_2; i.e., a clean fuel to be burnt in a GT for power production. Methane reforming improves heating value via thermo-chemical conversion into H_2 [34]. The GT generates waste heat, which is recovered in a HRSG to produce superheated HPS increasing power generation via steam-turbines of a Rankine-Cycle.

2.1.2. Properties of pure ionic-liquid [Bmim][NTf_2]

The use of [Bmim][NTf_2] as a physical solvent in the PCC step of ATR-GTW process is proposed as an alternative to conventional aqueous-MEA absorption. The IL [Bmim][NTf_2] is selected for this purpose due to its characteristics as a physical solvent for CO_2 capture. Liu et al. [26] considered [Bmim][NTf_2] as the best IL for high-pressure CO_2 absorption via an IL screening procedure based on CO_2 solubility, viscosity, and toxicity. Constant properties and temperature-dependent properties of pure IL [Bmim][NTf_2] are listed in Tables 1 and 2 from Barbosa et al. [29] and Ge et al. [35].

2.1.3. Thermodynamic modeling of ionic-liquid [Bmim][NTf_2] and gas solutes systems

The implementation of PCC-IL in Aspen-Plus requires the addition of IL as a new pure component as well as its parameters and properties. Additionally, NRTL binary interaction parameters for IL-solute pairs (IL-H_2, IL-CO_2, IL-CO, IL-N_2, IL-CH_4, IL-H_2O, IL-C_2H_6) are necessary for VLE modeling in absorption and stripping operations. Eq. (5) represents the VLE equation of species *i*; where $\widehat{f}_i^V$ and $\widehat{f}_i^L$ stand for species *i* fugacities in vapor and liquid phases. Eq. (5) is rewritten as Eq. (6), where *P* is the pressure, $y_i$and $x_i$represents species *i* vapor and liquid mol fractions, $\widehat{\varphi}_i^V$, $f_i^0(T,P)$ and $\widehat{\gamma}_i^L$ respectively stand for species *i* vapor fugacity coefficient, standard state fugacity at (T,P), and liquid activity coefficient.

$$\widehat{f}_i^V = \widehat{f}_i^L \quad (5)$$

$$P \cdot y_i \cdot \widehat{\varphi}_i^V = f_i^0(T,P) \cdot \widehat{y}_i^L \cdot x \quad (6)$$

Fugacities of supercritical species CH_4, C_2H_6, CO, CO_2, N_2, O_2 and H_2 in IL phase are represented using the respective IL Henry constants as standard state fugacities dependent of temperature and pressure in Eq. (6). IL Henry constants of O_2, N_2, CO and H_2 are modeled as approximately independent of pressure; i.e., the respective infinite dilution Poynting corrections are not present due to lack of partial molar volumes at infinite IL dilution. For CO_2, CH_4 and C_2H_6 the Henry constants are complete [29]. Thus, supercritical IL Henry constants are represented in Eqs. (7a) and (7b) for species *i*, where *T(K)*, *P(bar)* and H_i^{IL}*(bar)* is the IL Henry constant of species *i* written with parameters C_{i1} to C_{i6}. Henry constant parameters are shown in Table 3 for all supercritical solutes in

Table 3
Parameters for Henry constants of supercritical solutes in [Bmim] [NTf_2].

Parameter	$i \equiv CH_4$	$i \equiv C_2H_6$	$i \equiv CO_2$	$i \equiv CO$	$i \equiv N_2$	$i \equiv O_2$	$i \equiv H_2$
C_{i1}	*0.0630*	*0.0615*	*10.6511*	*−1.0218*	*10.969*	*10.969*	*50.83*
C_{i2} *(K)*	*1.89E-04*	*9.10E-04*	*−0.3393*	*−0.3391*	*0.122879*	*0.122879*	*0.664*
C_{i3}	*0.9170*	*0.2143*	*2.2453*	*0.8499*	*−0.701233*	*−0.701233*	*−9.77*
C_{i4} *(K^{-1})*	*0.0016*	*0.0114*	*0.0049*	*0.0064*	*0*	*0*	*0.04*
C_{i5} *(K. bar^{-1})*	*1.7830*	*−3.20E-05*	*1.2194*	*0*	*0*	*0*	*0*
C_{i6} *(bar^{-1})*	*−0.0049*	*−0.0087*	*−0.0039*	*0*	*0*	*0*	*0*
T Range (K)	*313–449*	*283–323*	*313–449*	*295*	*314–353*	*314–353*	*333–449*
P Range (bar)	*15–105*	*1–13*	*4–108*	*1–93*	*11.9–56.1*	*11.9–56.1*	*28.2–154.3*
Source	[29]	[29]	[29]	[36]	[37]	[37]	[38]

Table 4
Simulation assumptions: ATR gas-to-wire with PCC-MEA.

Item	Description	Assumption
{S1}	*Thermodynamic Modeling*	*Overall (except PCC): PR-EOS; PCC-MEA: Aspen Amine-Package;*
{S2}	*NG Feed (%mol composition)*	*1.89 MMSm^3/d; P*=60 bar; *T*=35°C; CH_4=85%mol, C_2H_6=6%mol, C_3H_8=3%mol, C_4H_{10}=0.5%mol, i-C_4H_{10}=0.5%mol, C_5H_{12}=0.25%mol, i-C_5H_{12}=0.25%mol, C_6H_{14}=0.5%mol, CO_2=3%mol.
{S3}	*Air (ATR, GT, CW-Tower)*	*T*=25°C; *P*= 1.013 bar; *Relative-Humidity*=60%; *Dry-Basis:* N_2=79%mol, O_2=21%mol.
{S4}	*ATR Reactor*	*P*=60 bar; *Model: Aspen Adiabatic Gibbs-Reactor; Steam/NG Molar Ratio*≈1.54; *Air/NG Molar Ratio*≈3.83
{S5}	*Steam*	*Saturated MPS: P*=60 bar, *T*=275.6°C; *Saturated HPS: P*=130 bar, *T*=330.9°C; *Stg#1 Steam-Turbine Superheated HPS: P*=129 bar, *T*=825°C; *Stg#2 Steam-Turbine Superheated HPS: P*=129 bar, *T*=808°C.
{S6}	*WGS Reactors*	$P^{HT\text{-}WGS}$=57.5 bar, $P^{LT\text{-}WGS}$=56.5 bar; $Conversion^{HT\text{-}WGS}$=70%, $Conversion^{Global}$=99%; *Model: Aspen Adiabatic Conversion-Reactor*
{S7}	*PCC-MEA*	*Theoretical Stages:* $Stages^{Absorber}$=20, $Stages^{Stripper}$=10. $P^{Absorber}$=55 bar; $P^{Stripper}$=1.013 bar. *Fresh Solvent: Water*=70%w/w; *MEA*=30%w/w; *Capture-Ratio: CR* ~ 10$kg^{SOLVENT}/kg^{CO2}$; *Stripping Heat-Ratio: HR* ~ 200kJ/molCO_2;
{S8}	*CO_2 Compression (Intercooled)*	P^{Final}=170 bar; T^{Final} =40°C (Liquid CO_2); *CO_2-EOR purity:* ≥ 85%mol; *Stage Compression-Ratio*≈3.4.
{S9}	*Gas-Turbine Combustor*	*P*=55 bar; *Adiabatic Operation; Air/H_2-Fuel Molar Ratio*≈1.59; *Maximum CO_2 Content: 3.5%mol Model: Aspen Adiabatic Gibbs-Reactor.*
{S10}	*Gas-Turbine Expander*	P^{Inlet} =55 bar; P^{Outlet} =5 bar;
{S11}	*Steam-Turbine*	*1st Stage:* P^{Inlet} =130 bar; P^{Outlet} =10 bar; *2nd Stage:* P^{Inlet} =10 bar; P^{Outlet} =0.1 bar;
{S12}	*HRSG and Rankine-Cycle*	P^{Pump}=130 bar; $T^{Flue\text{-}Gas}$=40°C.
{S13}	*CW CW-Tower*	*CW:* T^{Inlet}=35°C, P^{Inlet} =4 bar, T^{Outlet}=50°C, P^{Outlet}=3.5 bar; $Blowdown^{Flow\text{-}Rate}$=$Evaporation^{Flow\text{-}Rate}$.
{S14}	*Heat Exchangers*	$\Delta T^{Approach}$=50°C (gas-gas); $\Delta T^{Approach}$=10°C (liquid-liquid); ΔP^{GAS}=0.5 bar; ΔP^{LIQ}=0.2 bar;
{S15}	*Adiabatic Efficiencies*	*Pumps*=80%; *Compressors*=80%; *Gas-Turbine*=80%; *Steam-Turbines*=80%;
{S16}	*Electricity*	*Priority=Internal Demand; Surplus Exported*

[Bmim][NTf_2]. Henry constants for CH_4, C_2H_6, and CO_2 were obtained directly from Barbosa et al. [29], while the counterparts for CO, N_2, O_2 and H_2 were fitted versus *T(K)* from IL-solute Henry constants gathered elsewhere (Table 3). Inserting Henry constants as standard state fugacity of supercritical solutes in Eq. (6) gives Eq. (8), while Eq. (6) becomes Eq. (9) for subcritical species (H_2O, IL, hydrocarbons C_3+) which adopt the standard state fugacity as the pure liquid fugacity at (*T,P*) based on vapor pressures and Poynting corrections [29]. In IL operations, vapor fugacity coefficients ($\widehat{\phi}_i^V$) in Eqs. (8) and (9) were calculated with the Redlich–Kwong Equation-of-State (RK-EOS) as adopted by Liu et al. [26]. Activity coefficients ($\widehat{\gamma}_i^L$) were calculated via NRTL liquid solution model [26], whose activity coefficients were appropriately converted to the due standard states (Henry Law for supercritical species or Lewis-Randall Rule for subcritical species).

$$\ln H_i^{IL}(T,P) = C_{i1} + C_{i2}/T + C_{i3}.\ln T + C_{i4}.T + (C_{i5}/T + C_{i6}).\left(P - P_{IL}^{Sat}(T)\right) \quad , \quad i = CO_2,\ CH_4,\ C_2H_6 \tag{7a}$$

$$\ln H_i^{IL} = C_{i1} + C_{i2}/T + C_{i3}.\ln T + C_{i4}.T \quad , \quad i = H_2,\ CO,\ N_2,\ O_2 \tag{7b}$$

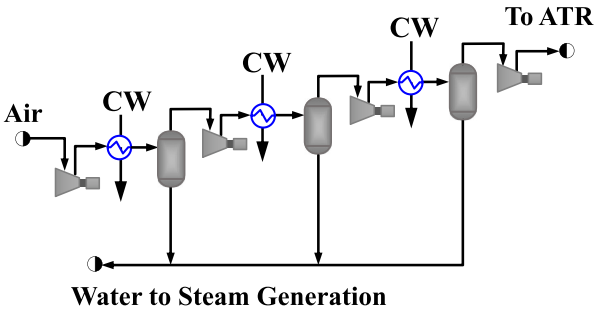

Fig. 2. ATR air compression train.

$$P.\,y_i.\,\widehat{\varphi}_i^{\,V} = H_i^{IL}(T,P).\widehat{\gamma}_i^{L}.x_i, i = CO_2 CO, H_2, N_2, O_2, CH_4, C_2H_6 \tag{8}$$

$$P.\,y_i.\,\widehat{\varphi}_i^{\,V} = f_i^{L}(T,P).\,\widehat{\gamma}_i^{L}.x_i \quad , \quad i = IL,\ H_2O,\ C_3^+ \tag{9}$$

Binary NRTL parameters IL-H_2O, IL-CO_2, IL-CH_4, IL-C_2H_6 and IL-C_3+ were gathered from Barbosa et al. [29]. The other solute binary NRTL parameters (i.e., IL-CO, IL-N_2, IL-O_2 and IL-H_2) are probably not available in the literature, but they are expected to be small and nearly zero in this application. So, they were considered as such; i.e., the individual behavior of such solutes in a binary IL-solute phase is considered an ideal solution with Henry Law solute standard state (similar approximations were adopted elsewhere [28]). Binary RK-EOS interaction parameters are used as existing in the Aspen-Plus data library, with the parameters of IL pairs set to zero as IL is practically absent in the vapor phase.

2.2. Autothermal steam-reforming gas-to-wire with post-combustion Aqueous-MEA capture: design and simulation

A large-scale ATR-GTW plant with PCC-MEA - so-called Base-Case - was designed and simulated following Fig. 1. The chosen scale corresponds to a NG feed of *1.89 MMSm^3/d* containing C_1–C_6 hydrocarbons. The NG feed is supposed dehydrated, desulfurized and with low CO_2 content. NG specifications as well as all simulation assumptions are presented in Table 4.

2.2.1. Air compression

Air to ATR reactor is compressed to 60 bar in a 4-staged intercooled compression train as shown in Fig. 2. Condensed water from knock-out vessels is used for steam generation. Each stage operates with P^{Outlet}/P^{Inlet}=3.3 and T^{Outlet}=40°C from intercoolers, which are cooled with cooling-water (CW). The last stage does not have aftercooler.

2.2.2. Autothermal reforming reactor

NG feed is mixed with MPS (Steam/NG molar ratio *1.545*) and preheated to ≈400°C. Compressed air is also preheated and feed the ATR reactor with the NG-MPS stream as schematized in Fig. 3. Due to its high temperature the ATR reactor is modeled as a chemical equilibrium reactor (Gibbs-Reactor).

The effluent gas leaves the reformer at ≈1000°C and is cooled in boilers that generate saturated HPS and MPS. The ATR effluent is also used for preheating both ATR feed streams NG + MPS and compressed air [39]. The final temperature of the raw-syngas is ~ 295°C, appropriated as WGS inlet temperature. The heat generated in the ATR is primarily used to vaporize high-pressure condensate (HPL) producing saturated HPS at 130 bar. In a second boiler medium-pressure condensate (MPL) boils to saturated MPS at 60 bar. Saturated HPS is used exclusively for power production being firstly superheated in the HRSG with GT exhausts and then sent to steam-turbines in the Rankine-Cycle. A part of MPS is fed to the ATR reactor and the rest is used as heat source in the PCC.

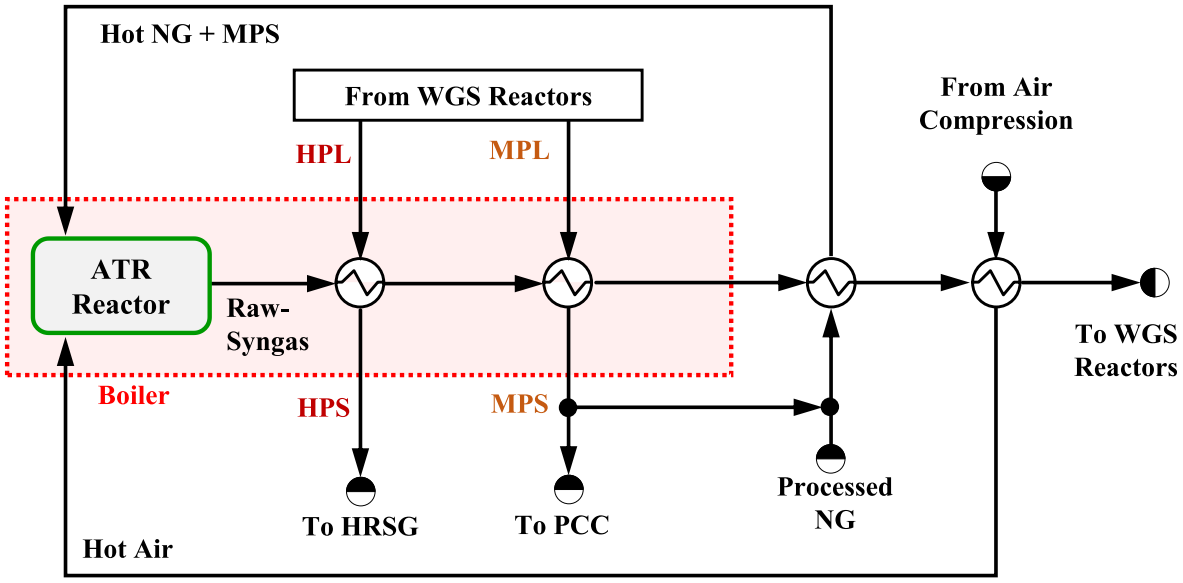

Fig. 3. ATR reactor and HPS/MPS loops (HPL and MPL represent high-pressure and medium-pressure condensates).

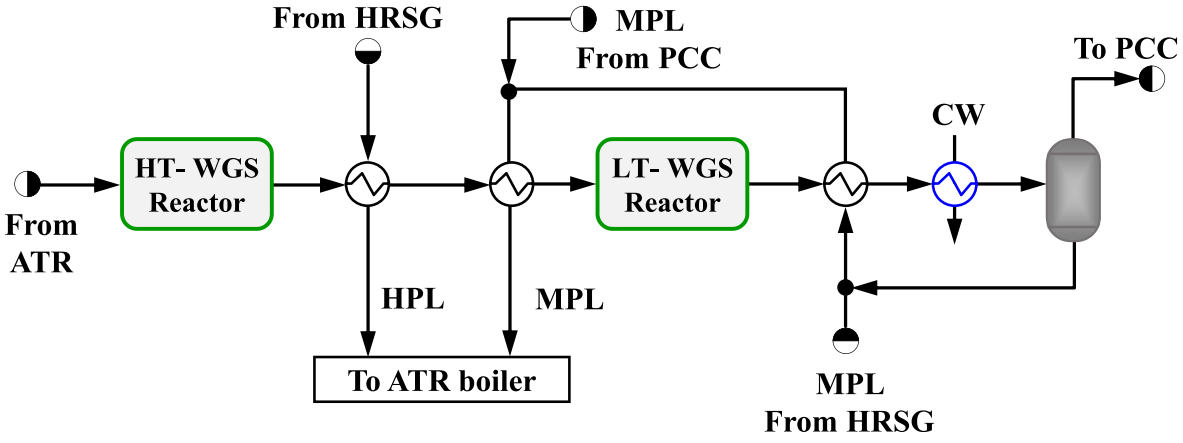

Fig. 4. High-temperature and low-temperature WGS reactors.

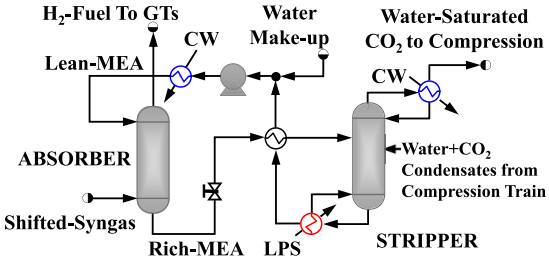

Fig. 5. PCC-MEA CO_2 capture.

2.2.3. Water-gas shift reactors

The high CO content of the ATR effluent is converted into CO_2 and H_2 in two serial adiabatic WGS reactors in Fig. 4. WGS reaction Eq. (4) is mildly exothermic. The first WGS reactor is fed with ATR effluent at $T \sim 295°C$ producing shifted-syngas at high-temperature $T \sim 377°C$ (HT-WGS) which is cooled while preheats condensates HPL/MPL. The second WGS reactor (LT-WGS) is fed with low-temperature gas at $T \sim 190°C$ producing shifted-syngas at $T \sim 210°C$. LT-WGS effluent preheats MPL condensate and is cooled with CW producing water condensate in a knock-out vessel which is recovered for steam generation (Fig. 4).

2.2.4. Pre-combustion capture and carbon dioxide compression

Before being fired in the GT's, H_2-Fuel is decarbonated in the PCC plant, which selectively captures CO_2 from the shifted-syngas. The ATR-GTW with conventional PCC-MEA absorbs CO_2 with aqueous-MEA *30% w/w*. Fig. 5 depicts the PCC-MEA comprising absorber and solvent stripper.

Shifted-syngas ($T=40^oC, P=55$ bar) enters the bottom of the absorber counter-currently contacting Lean-MEA and producing decarbonated gas at the top – so-called H_2-Fuel. Rich-MEA leaves as absorber bottoms and, after being preheated by hot Lean-MEA, feeds the low-pressure stripper. All condensates from compression of water-saturated CO_2 return with water and CO_2 to the stripper reducing water make-up, which is necessary to compensate water losses in H_2-Fuel and in the final compressed CO_2-EOR product. PCC-MEA is designed to capture CO_2 in the shifted-syngas with two key parameters: capture-ratio (*CR*) and heat-ratio (*HR*); *CR* expresses the weight of fresh solvent to capture *1* kg^{CO2}, while *HR* is the heat demanded to strip *1* kg^{CO2}. For *30%w/w* aqueous-MEA $CR \sim 10kg^{Solvent}/kg^{CO2}$ and $HR \sim 200kJ/molCO_2$ [40]. PCC-MEA executes temperature-swing and pressure-swing absorption; i.e., to achieve the desired solvent regeneration, the stripping requires not only heating, but also depressurization to $P=1.013$ bar. The heat for solvent regeneration is supplied by saturated MPS, which boils the reboiler at $T \sim 103°C$. The water-saturated stripped CO_2 follows to a

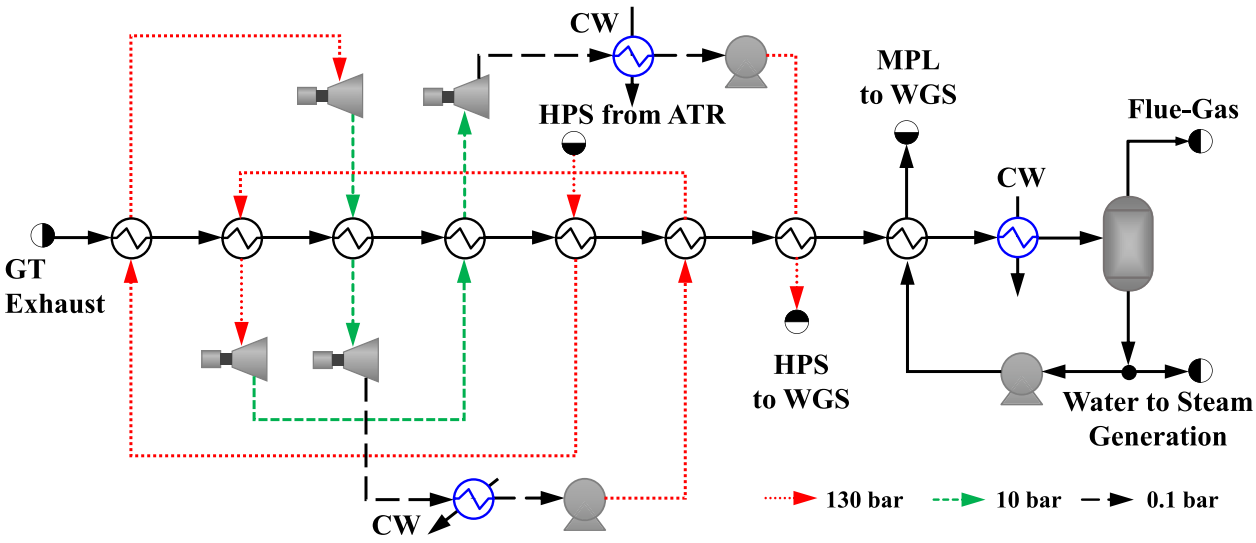

Fig. 6. Heat-recovery steam-generator and steam Rankine-Cycle for power generation.

compression train with three intercooled centrifugal stages. Each stage operates with $P^{Outlet}/P^{Inlet}=3.4$, intercooled to $T^{Outlet}=40^{o}C$, whose water-CO_2 condensates are collected in knock-out drums and returned to the stripper to avoid water-CO_2 losses. The CO_2 stream is compressed again in another stage until liquefaction to be exported as CO_2-EOR product. The H_2-Fuel leaving the absorber is basically H_2+N_2 to be burn with air in gas-turbines.

2.2.5. Hydrogen combined-cycle: gas-turbine, heat-recovery steam-generator and steam Rankine-Cycle

The H_2-Fuel from PCC is burnt in gas-turbines with air/fuel molar ratio of ~1.59. Compressed air comes at 55 bar from a single-stage axial compressor. The combustion-chamber provides hot flue-gas at ≈1500°C, which is adiabatically expanded for power generation. GT effluent is sent to the HRSG coupled to Rankine-Cycle for power generation via steam-turbines (Fig. 6).

Saturated HPS from the boiler (T=330.9°C) is superheated in the first exchanger (Fig. 6) and expanded in stage#1 steam-turbine to 10 bar. After re-heated, this steam expands in stage#2 steam-turbine to 0.1 bar. HPS temperature ensures no condensation at turbine outlet. The expanded steam is condensed and pumped to P=130 bar in order to repeat the generation scheme, however starting from the second exchanger. After the stage#2 of expansion, the condensate is pumped again to P=130 bar and recovers heat from HT-WGS outlet. The flue-gas from the GT and HRSG carries a residual heat used to preheat part of the condensate from flue-gas cooling which produces MPS to ATR, the remaining is used for steam generation or other make-up needs. CW guarantees flue-gas final temperature of 40°C.

2.3. Simulation assumptions

Table 4 summarizes simulation assumptions for the ATR-GTW with PCC-MEA.

2.4. Autothermal reforming gas-to-wire using ionic-liquid pre-combustion capture

The ATR-GTW with PCC-IL - so-called IL-Case - was implemented in Aspen-Plus, which allows not only creating new components, such as IL, but also to introduce complex thermodynamic and transport properties. This new temperature-swing PCC-IL plant performs CO_2 removal, releasing a high-pressure CO_2 stream. PCC-IL differs from PCC-MEA mainly in the stripping stage. While PCC-MEA uses a stripper column to promote solvent regeneration at atmospheric pressure, PCC-IL accomplishes the IL regeneration using two adiabatic flash-strippers at high-temperature, allowing stripping at high-pressure, as shown in Fig. 7. To increase absorption, it is proposed an additional cooling of the gas feed to 25°C with chilled-water.

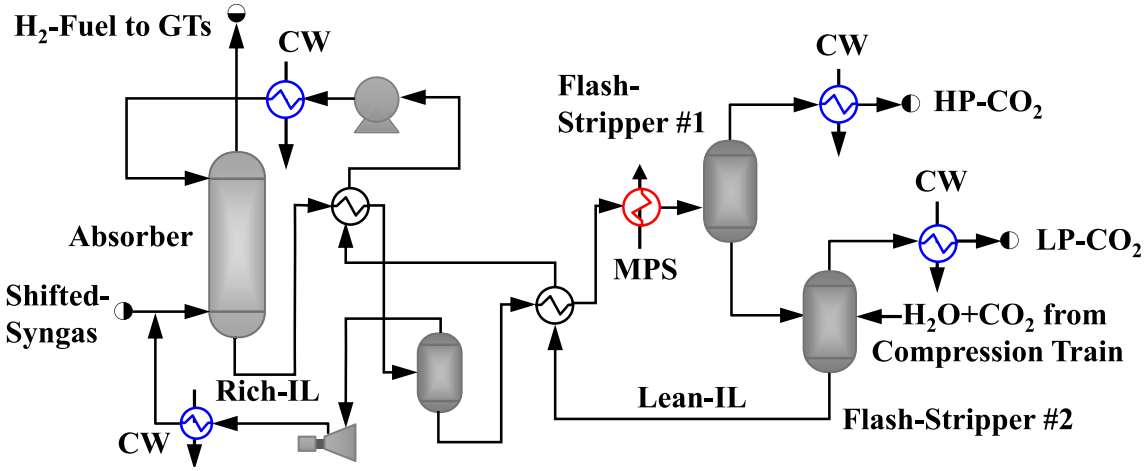

Fig. 7. PCC-IL for shifted-syngas decarbonation.

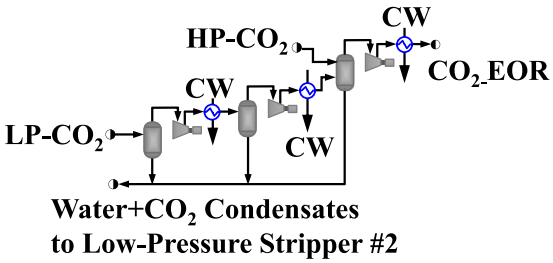

Fig. 8. PCC-IL CO_2 compression train (LP = low-pressure, HP = high-pressure).

Table 5
Simulation assumptions: PCC-IL.

Item	Description	Assumption
{S17}	PCC-IL Thermodynamic Modeling	Vapor-Phase:RK-EOS, Liquid-Phase:NRTL, Solutes Standard-State: Henry Law.
{S18}	Fresh IL Solvent	100% [Bmim][NTf_2].
{S19}	Absorber	P=60 bar; Theoretical Stages: 15; Capture-Ratio: CR=40 kg^{IL}/kg^{CO2}.
{S20}	Temperature-Swing Strippers	Adiabatic-Stripper#1: P=50 bar, T^{Inlet}=265°C; Adiabatic-Stripper#2: P=5 bar.
{S21}	Chilled-Water	T^{Inlet}=5°C, P^{Inlet} =4 bar; T^{Outlet}=15°C, P^{Outlet}=3.5 bar.

PCC-IL operates temperature-swing absorption. The shifted-syngas is fed to the absorber at the bottom (tray #15) while Lean-IL is fed at the top. Rich-IL is preheated with hot Lean-IL in two stages. The first heating increases IL temperature only to *130°C* partially stripping the absorbed gas in the pre-stripper (Fig. 7) at 55 bar. This pre-stripped gas returns to the absorber. The pre-stripping aims at purging part of the H_2 carried by IL, which increases the recovery of H_2-Fuel and lowers CO_2 compression power by reducing the H_2 content in the CO_2-rich product [28]. The second heating with Lean-IL rises the Rich-IL temperature near to the desired stripping temperature, which is finally achieved at *T=265°C* by a last MPS heating. This level of heating does not affect the long-term IL integrity since Meine et al. [41] report thermal decomposition of [Bmim][NTf_2] initiating at *461°C*.

CO_2 stripping occurs in two stages. Rich-IL is sent to high-pressure adiabatic flash Stripper#1 at *P*=50 bar, where a greater CO_2 fraction is stripped at *T=265°C*. The partially stripped IL expands to adiabatic flash Stripper#2 at *P*=5 bar. This configuration generates two CO_2-rich streams: HP-CO_2 at 50 bar and LP-CO_2 at 5 bar, which are sent to the compression train (Fig. 8). Table 5 shows simulation assumptions for PCC-IL, while assumptions for the other IL-Case operations are the same already adopted for the Base-Case (Table 4).

2.5. Economic analysis

ATR-GTW with PCC-IL and the PCC-MEA counterpart are investigated on economic grounds. Process simulation of both cases provides equipment data for sizing and design, which allows estimating the fixed capital investment (*FCI,MMUSD*). *FCI* and other economic variables cost of manufacturing (*COM,MMUSD/y*), revenues (*REV,MMUSD/y*) and net present value (*NPV,MMUSD*) are estimated via Turton et al. [42] in Appendix A.

3. Results and discussion

Technical and economic performances of ATR-GTW with PCC-IL and the PCC-MEA counterpart are discussed as follows.

Table 6
Product streams of ATR and WGS reactors.

	ATR	HT-WGS	LT-WGS
T (°C)	*1000*	*377*	*272*
P (bar)	*60.0*	*57.5*	*56.5*
% CH_4 [a]	*0.24*	*0.24*	*0.24*
%C_2+ [b]	*0.00*	*0.00*	*0.00*
%CO_2	*4.7*	*11.89*	*14.87*
%CO	*10.26*	*3.07*	*0.1*
%H_2O	*21.28*	*14.09*	*11.12*
% N_2	*38.19*	*38.19*	*38.19*
% O_2	*0.00*	*0.00*	*0.00*
% H_2	*25.33*	*32.52*	*35.49*

[a] %mol compositions.
[b] Ethane and heavier alkanes.

Table 7
Main PCC-MEA streams.

	Shifted-Syngas	H_2-Fuel	Stripped-CO_2	CO_2-EOR
T (°C)	*40*	*40*	*40*	*40*
P (bar)	*55*	*55*	*1.013*	*170*
Flow rate (t/h)	*460.5*	*293.8*	*172.6*	*167.0*
%CH_4 [a]	*0.36*	*0.43*	*0.00*	*0.00*
%C_2+ [b]	*0.00*	*0.00*	*0.00*	*0.00*
%CO_2	*16.74*	*0.00*	*92.58*	*99.71*
%CO	*0.06*	*0.08*	*0.00*	*0.00*
%H_2O	*0.16*	*0.15*	*7.41*	*0.27*
%N_2	*43.02*	*51.66*	*0.00*	*0.00*
%O_2	*0.00*	*0.00*	*0.00*	*0.00*
%H_2	*39.70*	*47.68*	*0.00*	*0.00*
%MEA	*0.00*	*0.00*	*0.00*	*0.00*

[a] %mol compositions.
[b] Ethane and heavier alkanes.

3.1. Technical analysis

From the NG feed of *1.89 $MMSm^3/d$*, the ATR unit produces raw-syngas with *10.*3 mol% of CO and *25.*3 mol% of H_2. The product leaves the reformer at ≈*1000°C* and provides heat to produce saturated HPS/MPS in the subsequent boilers and to preheat the ATR feed streams. After being cooled to *295°C* the raw-syngas is sent to the WGS reactors, where H_2 content is increased to *35.*49 mol% and cooled down to PCC temperature. The main product streams of ATR and WGS reactors are detailed in Table 6.

The temperature for the PCC step depends on the case. In PCC-MEA, which performs chemical-absorption, the LT-WGS outlet is cooled to *T=40°C*, a value reasonable to aqueous-MEA capture that demands not too low temperatures for kinetic reasons. After cooled, the LT-WGS product generates an aqueous condensate, which is removed and the remaining gas stream (shifted-syngas) has *39.70%mol* and *16.74%mol* of H_2 and CO_2, respectively. PCC-MEA absorption required 1671 t/h of Lean-MEA for achieving the required CO_2 content in the H_2-Fuel stream (Table 4, {S8}). H_2-Fuel (*T=40°C*, *P*=55 bar) leaves the absorber practically free of CO_2 and with *47.68%mol* H_2. The specified *HR* (Table 4, {S7}) leads to a reasonable stripper duty of 190 MW to provide a CO_2-rich stream – so-called Stripped-CO_2 – at *T=40°C* and *P=1.*013 bar. After the compression train, the CO_2 stream is dehydrated and liquefied (*T=40°C, P*=170 bar*)* in the aftercooler, reaching a density of *623.*31 kg/m^3. Table 7 summarizes PCC-MEA feed and products.

PCC-IL gas feed, on the other hand, is cooled to *T=25°C* achieving *39.70%mol* of H_2 and *16.74%mol* of CO_2. IL absorption required 6684 t/h of Lean-IL (Table 5, {S19}) to produce a H_2-Fuel with *3.4%mol* CO_2. The two strippers produce two CO_2-rich streams, LP-CO_2 and HP-CO_2. HP-CO_2 represents *90%* of all CO_2 stripped in PCC-IL, emphasizing the importance of high-pressure stripping, which implies significant power savings in the subsequent compression step. After two compression stages, the combined CO_2 stream is sent to the final intercooled

Table 8
Main PCC-IL streams.

	Shifted-Syngas	H_2-Fuel	HP-CO_2	LP-CO_2	CO_2-EOR
T (°C)	*25*	*25*	*265*	*267*	*40*
P (bar)	*55*	*55*	*50*	*5*	*170*
Flow rate (t/h)	*460.5*	*315.4*	*125.1*	*17.4*	*141.0*
%CH_4 [a]	*0.36*	*0.39*	*0.18*	*0.25*	*0.20*
%C_2+ [b]	*0.00*	*0.00*	*0.00*	*0.00*	*0.00*
%CO_2	*16.75*	*3.44*	*88.71*	*80.38*	*89.73*
%CO	*0.06*	*0.08*	*0.07*	*0.39*	*0.11*
%H_2O	*0.07*	*0.00*	*1.76*	*7.79*	*0.22*
%N_2	*43.05*	*49.62*	*6.32*	*11.11*	*7.09*
%O_2	*0.00*	*0.00*	*0.00*	*0.00*	*0.00*
%H_2	*39.74*	*46.47*	*2.95*	*0.09*	*2.66*
%[Bmim][NTf_2]	*0.00*	*0.00*	*0.00*	*0.00*	*0.00*

[a] %mol compositions.
[b] Ethane and heavier alkanes.

Table 9
Power and utilities consumption/production of both ATR-GTW alternatives.

Equipment/System	Consumption/Production*	
	Base-Case	IL-Case
Power (MW)		
Gas-Turbine	*279.86**	*286.85**
Steam-Turbines	*96.21**	*146.29**
Air Compression (ATR)	*58.91*	*58.91*
Air Compression (Gas-turbine)	*135.65*	*138.03*
Pumps (HRSG + CW)	*4.57*	*10.25*
PCC (Compression + Pumping)	*12.45*	*2.88*
Power Demand	*211.58*	*210.07*
Gross Power Produced	*376.07**	*433.13**
Net Power	*164.49*	*223.06*
Power Exported	*43.7%*	*51.5%*
Utilities (t/h)		
MPS	*376.8*	*166.2*
HPS	*85.0*	*135.0*
CW	*36,594.0*	*37,559.3*

compression stage, where it is liquefied as the CO_2-EOR stream (density of *512.*89 kg/m^3). Table 8 presents data for PCC-IL feed and product streams.

As seen in Table 8, CO_2-EOR stream from PCC-IL has a lower CO_2 purity and a lower flow rate – and a lower density reflecting its inferior CO_2 content – than the PCC-MEA analogues (Tables 7 and 8). The underlying reason has to do with the higher CO_2 selectivity from chemical-absorption and easy CO_2 capture at high-pressure performed by PCC-MEA which recovered ≈100% of CO_2 from shifted-syngas. Nevertheless, the somewhat inferior decarbonation performance of PCC-IL is still sufficient to recover 77% of CO_2 from the shifted-syngas producing an 89.73%mol CO_2 stream to EOR. This establishes IL-based ATR-GTW as a viable route to clean power production. Evidently, PCC-IL, which performs physical-absorption, exhibits lower CO_2 selectivity than PCC-MEA with its chemical-absorption enhanced by high-pressure. The leverage of PCC-IL does not lie only on its CO_2 selectivity (which is sufficiently high), but also on its capability to generate high-pressure stripped CO_2 strongly decreasing the subsequent compressor costs and investment, helping to increase the annual-profit of IL-based ATR-GTW over the analogous process with PCC-MEA which has to compress CO_2 from 1 bar up to 170 bar. But there are still more advantages of PCC-IL. In terms of energy, PCC-IL demands a higher temperature (*T=265°C*) for CO_2 stripping than PCC-MEA, however the heat requirement is expressively lower: only *34.*6 MW. The 5.5-fold reduction is achieved due to the weaker physical interaction IL-CO_2, which requires lower energy to release the physically absorbed CO_2. Heat consumption of PCC-IL decreases MPS demand and improves power production by increasing HPS availability. This impact is remarkable in the increase of *26.2%* in power exportation relatively to the ATR-GTW with PCC-MEA. Table 9 reports

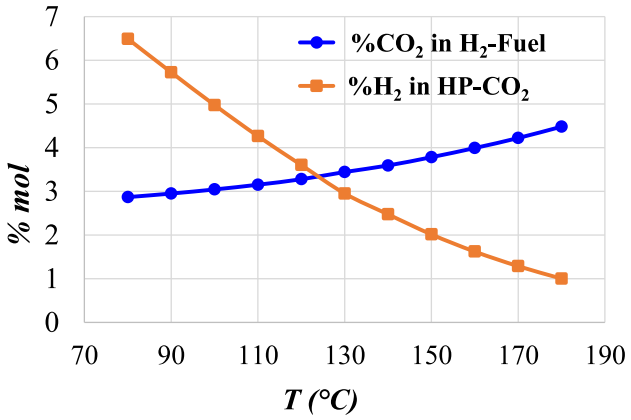

Fig. 9. PCC-IL: CO_2 in H_2-Fuel and H_2 in HP-CO_2 versus pre-stripper temperature.

Table 10
Economic summary of both ATR-GTW alternatives.

Economic Parameter	Base-Case	IL-Case
FCI (MMUSD)	*630.6*	*871.3 (+38.2%*[a]*)*
COM (MMUSD/y)	*199.0*	*248.7 (+25.0%*[a]*)*
REV (MMUSD/y)	*256.5*	*349.4 (+36.2%*[a]*)*
NPV (MMUSD)	*152.7*	*390.2 (+155%*[a]*)*

[a] Relative to Base-Case.

power consumption and power exportation (surplus) for both Base-Case (with PCC-MEA) and IL-Case (with PCC-IL).

3.1.1. *Sensitivity analysis of ionic-liquid capture pre-stripper temperature*

A sensitivity analysis was conducted to evaluate the best preheating temperature in the pre-stripping of PCC-IL which returns some H_2 to the IL absorber feed. The analysis was performed varying the Rich-IL temperature after the preheating from *80* to *180°C* to investigate its influence on CO_2 content of the decarbonated H_2-Fuel and on H_2 content of the high-pressure stripped HP-CO_2. Results are shown in Fig. 9 which unveils a trade-off between such contents of H_2 and CO_2. Lower temperatures tend to pre-strip a small flow rate of gas from Rich-IL, maintaining the CO_2 content near to the *3%mol* in H_2-Fuel, which is beneficial in terms of CO_2 capture. However, H_2 recuperation becomes unsatisfactory since its content is high in HP-CO_2 (*4–6%mol*). On the other hand, temperatures above *160°C* promote a most intense stripping observed as low H_2 content in the HP-CO_2 stream (*<2%mol*). Despite such reduced H_2 content entails gains in the CO_2 compression performance, the high CO_2 content in the H_2-Fuel (*>4%mol*), exceeds the established limit for CO_2 capture (Table 4, {S9}). All this said, the temperature initially assumed to the IL pre-stripper of *130°C* seems an adequate compromise, since CO_2 and H_2 contents are *3.4%mol* and *2.95%mol*, respectively in H_2-Fuel and HP-CO_2 streams.

3.2. *Economic analysis*

Economic performances of ATR-GTW with PCC-IL and the PCC-MEA counterpart are firstly evaluated in terms of fixed capital investment (*FCI*), cost of manufacture (*COM*), revenues (*REV*) and net present value (*NPV*) (30 years horizon) in Table 10. The ATR-GTW PCC-IL presents a *FCI 27.6%* higher than the PCC-MEA counterpart. Even though savings in some segments occur, such as stripper column elimination and reduction of CO_2-EOR compression power, the investment of the PCC-IL process is higher, especially in the HRSG. Due to increased power production, the generation system demands equipment with higher capacities (i.e., turbines, exchangers). The higher IL flow rate in PCC-IL

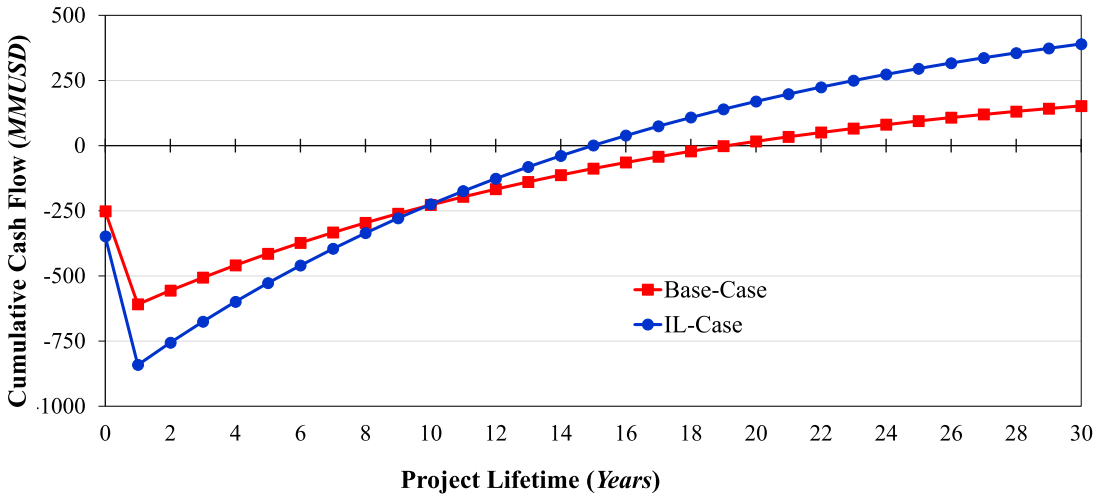

Fig. 10. NPV versus years: Base-Case and IL-Case.

also impacts negatively the *FCI*, due to elevated pump capacity and high heat exchangers area. This increase is also felt in *COM*, as well as the effect of using chilled-water to cool the PCC-IL feed temperature ($T=25°C$).

Even with the negative responses of *FCI* and *COM*, the greater *REV* response of ATR-GTW PCC-IL pushed it to outperform ATR-GTW PCC-MEA in terms of *NPV* response. This results from the greater electricity sales (*35.6%*) of ATR-GTW PCC-IL leading its *NPV* to attain more than twice the value achieved by the PCC-MEA counterpart. Fig. 10 depicts *NPV* of both cases for 28 operational years. Thanks to its superior *REV*, IL-Case has also lower payback-time (15 versus 20 years).

4. Conclusions

A new ATR-GTW with pre-combustion capture via temperature-swing IL absorption (PCC-IL) is presented as a better option than ATR-GTW with pre-combustion capture via conventional aqueous-MEA absorption. This new concept is based on temperature-swing physical-absorption with IL [Bmim][NTf_2] in the pre-combustion capture. The new ATR-GTW with PCC-IL was proven to be superior than the conventional ATR-GTW with PCC-MEA on both technical and economic grounds.

In the pre-combustion step, syngas is decarbonated to provide H_2-Fuel for combined-cycle power generation. It was shown that ATR-GTW with PCC-IL had the following technical advantages over the PCC-MEA counterpart: (i) high-pressure stripping entails a reduction of *4.3* times in CO_2 compression power for EOR utilization; (ii) CO_2 stripping requires *5.5* times less heat, reducing MPS demand proportionally and increasing HPS production with consequent increase of power production in the H_2 combined-cycle; (iii) consequently, HPS flow rate increases ≈*59%*, increasing proportionally the power production of the Rankine-Cycle and allowing to export ≈*36%* more electricity than the PCC-MEA counterpart.

Economically, the following leverages of the ATR-GTW with PCC-IL are highlighted relatively to the PCC-MEA counterpart: (i) ≈*36%* superior revenues due to higher production of electricity (*35.6%*) and CO_2-EOR sales; (ii) *NPV 155%* higher for *28 years* of operation, proving superior profitability; and (iii) payback-time is achieved *5 years* earlier than the PCC-MEA counterpart.

Based on the techno-economic performance of both cases, the PCC-IL process proved to be a promising alternative to substitute the conventional PCC-MEA process in the ATR-GTW plant. This is valid not only economically, but also due to attractive results on technical grounds. Thus, the new IL-based ATR-GTW plays an important role as CCS technology, since it performs low-emission via a cleaner hydrogen-fired power plant and delivers a liquified CO_2-rich stream to be properly used as EOR agent.

Author credit statement

Hudson Bolsoni Carminati: Software, Writing - original draft, Investigation, Validation, Formal analysis, Data curation, Visualization, Writing - review & editing.. José Luiz de Medeiros: Conceptualization, Methodology, Supervision, Writing - original draft, Writing - review & editing, Investigation, Validation, Visualization, Formal analysis, Funding acquisition, Project administration, Resources. Gustavo Torres Moure: Conceptualization, Methodology. Lara Costa Barbosa: Software, Investigation, Data curation.. Ofélia de Queiroz F. Araújo: Conceptualization, Methodology, Supervision, Funding acquisition, Project administration, Resources, Writing - review & editing.

Acknowledgements

Authors acknowledge financial support from Shell-Brasil S/A (041953/2017–76). JL de Medeiros and OQF Araújo also acknowledge support from CNPq-Brazil (311076/2017–3).

Appendix A. Economic Assumptions and Formulas

Process economic analysis follows Turton et al. [42] with economic assumptions in Table A1. Fixed capital investment (*FCI,MMUSD*) is the cost of installed equipment. Purchase cost of equipment is estimated in a reference condition and adjusted with design, pressure and material factors giving the bare module cost (C_{BM}) which is updated to the Reference Date (December-2017) using the *CEPCI=567.5* cost index [43]. C_{BM} for equipment capacities exceeding correlation limits are extrapolated via the *Six-Tenth Rule* in Eq. (A1), using capacity factor *CF* – e.g., power (machines), volume (vessels) and area (exchangers). C_{BM} is increased by *18%* for contingencies in Eq. (A2), where the number of equipment items (N_{EQ}) includes spares. The annual cost of manufacturing (*COM,MMUSD/y*), Eq. (A3), comprehends direct and fixed costs, the former encompassing costs of raw materials (*CRM,MMUSD/y*), utilities (*CUT,MMUSD/y*) and labor (*COL,MMUSD/y*). Gross annual-profit (*GAP,MMUSD/y*) and annual-profit (*AP,MMUSD/y*) are given in Eq. (A4) and Eq. (A5) using revenues (*REV,MMUSD/y*), income tax rate (*ITR,%)* and annual depreciation (*DEP,MMUSD/y)*. Eq. (A6) obtains

the net present value (*NPV*) where *N* is number of operational years and *i* is annual (percent) interest rate.

$$C_{BM} \Big/ C_{BM}^{Lim} = \left(CF/CF^{\mathrm{Lim}}\right)^{0.6} \tag{A1}$$

$$FCI = 1.18 \sum_{j=1}^{N_{EQ}} C_{BM}(j) \tag{A2}$$

$$COM = 0.18FCI + 2.73COL + 1.23(CUT + CRM) \tag{A3}$$

$$GAP = REV - COM \tag{A4}$$

$$AP = \begin{cases} GAP - (GAP - DEPR).ITR/100 & (GAP > DEPR) \\ GAP & (GAP \leq DEPR) \end{cases} \tag{A5}$$

$$NPV = -\left(0.4 + 0.6q^{-1}\right)FCI + AP\left(\sum_{k=2}^{N+2} q^{-k}\right) \quad , \quad q = (1 + i/100) \tag{A6}$$

Table A1
Economic Assumptions.

Item	Description	Assumptions
{E1}	*Equipment Material*	*Carbon Steel.*
{E2}	*Reference Date*	*December-2017; CEPCI=567.5* [43].
{E3}	*Raw Material Price*	*NG=2.82USD/MMBTU* [29].
{E4}	*Water-Utility Prices*	*Make-Up=0.003USD/m*^{3} [44]; *Chilled-Water=0.185USD/t* [42];
{E5}	*Product Prices*	*Electricity=154.7USD/MWh* [37]; CO_2^{EOR}*=65USD/t* [43].
{E6}	*Cost Parameters*	*COL=10%CRM; DEPR=10%FCI; ITR=34%; i=6%.*
{E7}	*Project Lifetime*	*Construction: 2 years (40%FCI+60%FCI); Operation: N=28 years.*
{E8}	*Plant Availability*	8000 h/y.
{E9}	*Catalyst*	*Density=0.6* kg/m^3*; Price=1USD/kg Weight Hourly Spatial Velocity: WHSV=1 (kg/h)/kg*
{E10}	*Solvent Prices*	*MEA=2USD/kg* [45]; *IL=20USD/kg* [29].

References

[1] Nazir SM, Cloete JH, Cloete S, Amini S. Efficient hydrogen production with CO_2 capture using gas switching reforming. Energy 2019;185:372–85. https://doi.org/10.1016/j.energy.2019.07.072.

[2] Taji M, Farsi M, Keshavarz P. Real time optimization of steam reforming of methane in an industrial hydrogen plant. Int J Hydrogen Energy 2018;43(29):13110–21. https://doi.org/10.1016/j.ijhydene.2018.05.094.

[3] Dong X, Pi G, Ma Z, Dong C. The reform of the natural gas industry in the PR of China. Renew Sustain Energy Rev 2017;73:582–93. https://doi.org/10.1016/j.rser.2017.01.157.

[4] Lemus RG, Duart JM. Updated hydrogen production costs and parities for conventional and renewable technologies. Int J Hydrogen Energy 2010;35(9):3929–36. https://doi.org/10.1016/j.ijhydene.2010.02.034.

[5] Gangadharan P, Kanchi KC, Lou HH. Evaluation of the economic and environmental impact of combining dry reforming with steam reforming of methane. Chem Eng Res Des 2012;90(11):1956–68. https://doi.org/10.1016/j.cherd.2012.04.008.

[6] Pashchenko D. First law energy analysis of thermochemical waste-heat recuperation by steam methane reforming. Energy 2018;143:478–87. https://doi.org/10.1016/j.energy.2017.11.012.

[7] Meerman JC, Hamborg ES, van Keulen T, Ramírez A, Turkenburg WC, Faaij APC. Techno-economic assessment of CO_2 capture at steam methane reforming facilities using commercially available technology. Int J Greenhouse Gas Contr 2012;9:160–71. https://doi.org/10.1016/j.ijggc.2012.02.018.

[8] Brigagão GV, de Medeiros JL, Araújo OQF. A novel cryogenic vapor-recompression air separation unit integrated to oxyfuel combined-cycle gas-to-wire plant with carbon dioxide enhanced oil recovery: energy and economic assessments. Energy Convers Manag 2019;189:202–14. https://doi.org/10.1016/j.enconman.2019.03.088.

[9] Andrei M, Sammarco G. Gas to wire with carbon capture and storage: a sustainable way for onsite power generation by produced gas. SPE Abu Dhabi Int. Petroleum Exhibition & Conference. Society of Petroleum Engineers 2017. https://doi.org/10.2118/188845-MS.

[10] Sengodan S, Lan R, Humphreys J, Du D, Xu W, Wang H, Tao S. Advances in reforming and partial oxidation of hydrocarbons for hydrogen production and fuel cell applications. Renew Sustain Energy Rev 2018;82(1):761–80. https://doi.org/10.1016/j.rser.2017.09.071.

[11] Abdulrasheed A, Jalil AA, Gambo Y, Ibrahim M, Hambali HU, Hamid MYS. A review on catalyst development for dry reforming of methane to syngas: recent advances. Renew Sustain Energy Rev 2019;108:173–93. https://doi.org/10.1016/j.rser.2019.03.054.

[12] Abdin Z, Zafaranloo A, Rafiee A, Mérida W, Lipiński W, Khalilpour KR. Hydrogen as an energy vector. Renew Sustain Energy Rev 2020:120. https://doi.org/10.1016/j.rser.2019.109620. 109620.

[13] Kayfeci M, Keçebaş A, Bayat M. Solar hydrogen production. Academic Press; 2019. p. 45–83. https://doi.org/10.1016/B978-0-12-814853-2.00003-5 [Chapter 3] - Hydrogen production.

[14] Speight JG. Gasification of unconventional feedstocks. Gulf Professional Publishing; 2014. p. 118–34. https://doi.org/10.1016/B978-0-12-799911-1.00005-4 [Chapter 5] - The Fischer–Tropsch Process.

[15] Soltani R, Rosen MA, Dincer I. Assessment of CO_2 capture options from various points in steam methane reforming for hydrogen production. Int J Hydrogen Energy 2014;39(35):20266–75. https://doi.org/10.1016/j.ijhydene.2014.09.161.

[16] Sharma I, Friedrich D, Friedrich T, Brandani S. Exploring the opportunities for carbon capture in modular, small-scale steam methane reforming: an energetic perspective. Int J Hydrogen Energy 2019;44:14732–43. https://doi.org/10.1016/j.ijhydene.2019.04.080.

[17] Park A, Kim YM, Kim JF, Lee PS, Cho YH, Park HS, Nam SE, Park YI. Biogas upgrading using membrane contactor process: pressure-cascaded stripping configuration. Separ Purif Technol 2017;183:358–65. https://doi.org/10.1016/j.seppur.2017.03.006.

[18] de Medeiros JL, Barbosa LC, Araújo OQF. Equilibrium approach for CO_2 and H_2S absorption with aqueous solutions of alkanolamines: theory and parameter estimation. Ind Eng Chem Res 2013;52(26):9203–26. https://doi.org/10.1021/ie302558b.

[19] Sreedhar I, Nahar T, Venugopal A, Srinivas B. Carbon capture by absorption – path covered and ahead. Renew Sustain Energy Rev 2017;76:1080–107. https://doi.org/10.1016/j.rser.2017.03.109.

[20] Aghaie M, Rezaei N, Zendehboudi S. A systematic review on CO_2 capture with ionic liquids: current status and future prospects. Renew Sustain Energy Rev 2018;96:502–25. https://doi.org/10.1016/j.rser.2018.07.004.

[21] Gassner M, Maréchal F. Thermo-economic process model for thermochemical production of Synthetic Natural Gas (SNG) from lignocellulosic biomass. Biomass Bioenergy 2009;33(11):1587–604. https://doi.org/10.1016/j.biombioe.2009.08.004.

[22] George G, Bhoria N, AlHallaq S, Abdala A, Mittal V. Polymer membranes for acid gas removal from natural gas. Separ Purif Technol 2016;158:333–56. https://doi.org/10.1016/j.seppur.2015.12.033.

[23] Barbosa LC, Nascimento MVC, Araújo OQF, de Medeiros JL. A cleaner and more sustainable decarbonation process via ionic-liquid absorption for natural gas with high carbon dioxide content. J Clean Prod 2020;(118421):242. https://doi.org/10.1016/j.jclepro.2019.118421.

[24] Zeng S, Zhang X, Bai L, Zhang X, Wang H, Wang J, Bao D, Li M, Liu X, Zhang S. Ionic-liquid-based CO_2 capture systems: structure, interaction and process. Chemieanlagen Verfahr 2017;117(14):9625–73. https://doi.org/10.1021/acs.chemrev.7b00072.

[25] Shiflett MB, Drew DW, Cantini RA, Yokozeki A. Carbon dioxide capture using ionic liquid 1-Butyl-3-methylimidazolium acetate. Energy Fuels 2010;24(10):5781–9. https://doi.org/10.1021/ef100868a.

[26] Liu X, Huang Y, Zhao Y, Gani R, Zhang X, Zhang S. Ionic liquid design and process simulation for decarbonisation of shale gas. Ind Eng Chem Res 2016;55(20):5931–44. https://doi.org/10.1021/acs.iecr.6b00029.

[27] Ma Y, Gao J, Wang Y, Hu J, Cui P. Ionic liquid-based CO_2 capture in power plants for low carbon emissions. Int J Greenhouse Gas Contr 2018;75:134–9. https://doi.org/10.1016/j.ijggc.2018.05.025.

[28] Zubeir LF, Lacroix MHM, Meuldijk J, Kroon MC, Kissc AA. Novel pressure and temperature swing processes for CO_2 capture using low viscosity ionic liquids. Separ Purif Technol 2018;204:314–27. https://doi.org/10.1016/j.seppur.2018.04.085.

[29] Barbosa LC, Araújo OQF, de Medeiros JL. Carbon capture and adjustment of water and hydrocarbon dew-points via absorption with ionic liquid [Bmim] [NTf_2] in offshore processing of CO_2-rich natural gas. J Nat Gas Sci Eng 2019;66:26–41. https://doi.org/10.1016/j.jngse.2019.03.014.

[30] Salvi BL, Panwar NL. Alternative fuels for transportation vehicles: a technical review. Renew Sustain Energy Rev 2013;25:404–19. https://doi.org/10.1016/j.rser.2013.04.017.

[31] Speight JG, Luque Rafael, Speight James G. Gasification for Synthetic Fuel Production. Cap. 10 - heavy hydrocarbon gasification for synthetic fuel production. Woodhead Publishing; 2015. p. 221–39. https://doi.org/10.1016/B978-0-85709-802-3.00010-2.

[32] Bergthorson JM, Thomson MJ. A review of the combustion and emissions properties of advanced transportation biofuels and their impact on existing and future engines. Renew Sustain Energy Rev 2015;42:1393–417. https://doi.org/10.1016/j.rser.2014.10.034.

[33] Pal DB, Chand R, Upadhyay SN, Mishra PK. Performance of water gas shift reaction catalysts: a review. Renew Sustain Energy Rev 2018;93:549–65. https://doi.org/10.1016/j.rser.2018.05.003.

[34] Gaber C, Demuth M, Prieler R, Schluckner C, Hochenauer C. An experimental study of a thermochemical regeneration waste heat recovery process using a reformer unit. Energy 2018;155:381–91. https://doi.org/10.1016/j.energy.2018.04.154.

[35] Ge R, Hardacre C, Jacquemin J, Nancarrow P, Rooney DW. Heat capacities of ionic liquids as a function of temperature at 0.1 MPa. Measurement and prediction. J Chem Eng Data 2008;53(9):2148–53. https://doi.org/10.1021/je800335v.

[36] Ohlin CA, Dyson PJ, Laurenczy G. Carbon monoxide solubility in ionic liquids: determination, prediction and relevance to hydroformylation. Chem Commun 2004;9:1070–1. https://doi.org/10.1039/B401537A.

[37] Anthony JL, Anderson JL, Maginn EJ, Brennecke JF. Anion effects on gas solubility in ionic liquids. J Phys Chem B 2005;109:6366–74. https://doi.org/10.1021/jp046404l.

[38] Raeissi S, Peters CJ. High pressure phase behaviour of methane in 1-butyl-3-methylimidazolium bis(trifluoromethylsulfonyl)imide. Fluid Phase Equil 2010;294(1-2):67–71. https://doi.org/10.1016/j.fluid.2010.03.021.

[39] Chiesa P. Advanced Power Plant Materials, Design and Technology. Chap. 15: advanced technologies for syngas and hydrogen (H_2) production from fossil-fuel feedstocks in power plants. In: Dermot roddy. Woodhead Publishing; 2010. p. 383–411. https://doi.org/10.1533/9781845699468.3.383.

[40] Araújo OQF, de Medeiros JL. Carbon capture and storage technologies: present scenario and drivers of innovation. Curr Opin Chem Eng 2017;17:22–34. https://doi.org/10.1016/j.coche.2017.05.004.

[41] Meine N, Benedito F, Rinaldi R. Thermal stability of ionic liquids assessed by potentiometric titration. Green Chem 2010;12(10):1711–4. https://doi.org/10.1039/C0GC00091D.

[42] Turton R, Bailie RC, Whiting WB, Shaeiwitz JA, Bhattacharyya D. Analysis, synthesis and design of chemical processes. 4thEd., vol. 13. USA: Prentice Hall; 2012. p. 978. 0-13-261812-0.

[43] Carminati HB, Milão RFD, de Medeiros JL, Araujo OQF. Bioenergy and full carbon dioxide sinking in sugarcane-biorefinery with post-combustion capture and storage: techno-economic feasibility. Appl Energy 2019;254:113633. https://doi.org/10.1016/j.apenergy.2019.113633.

[44] Milão RFD, Carminati HB, Araujo OQF, de Medeiros JL. Thermodynamic, financial and resource assessments of a large-scale sugarcane-biorefinery: prelude of full bioenergy carbon capture and storage scenario. Renew Sustain Energy Rev 2019;113:109251. https://doi.org/10.1016/j.rser.2019.109251.

[45] Alibaba. Monoethanolamine price. 56f84f56jsXYrr Accessed, https://www.alibaba.com/product-detail/MEA-99-5-min-Monoethanolamine-price_60300074199.html?spm=a2700.galleryofferlist.0.0. [Accessed 26 December 2019].